

Superzone gap formation and low lying crystal electric field levels in PrPd₂Ge₂ single crystal

Arvind Maurya,* S. K. Dhar, and A. Thamizhavel

Department of Condensed Matter Physics and Materials Science,

Tata Institute of Fundamental Research,

Homi Bhabha Road, Colaba, Mumbai 400 005, India.

(Dated: September 18, 2018)

Abstract

The magnetocrystalline anisotropy exhibited in PrPd₂Ge₂ single crystal has been investigated by measuring the magnetization, magnetic susceptibility, electrical resistivity and heat capacity. PrPd₂Ge₂ crystallizes in the well known ThCr₂Si₂-type tetragonal structure. The antiferromagnetic ordering is confirmed as 5.1 K with the [001]-axis as the easy axis of magnetization. A superzone gap formation is observed from the electrical resistivity measurement when the current is passed along the [001] direction. The crystal electric field (CEF) analysis on the magnetic susceptibility, magnetization and the heat capacity measurements confirms a doublet ground state with a relatively low over all CEF level splitting. The CEF level spacings and the Zeeman splitting at high fields become comparable and lead to metamagnetic transition at 34 T due to the CEF level crossing.

PACS numbers: 81.10.Fq, 75.30.Kz, 75.50.Ee, 75.10.Dg

I. INTRODUCTION

Praseodymium (Pr^{3+}), being a non-Kramer's ion exhibits a variety of interesting magnetic behaviour in its compounds. Pr^{3+} often orders magnetically with a doublet ground state, while it behaves as a Van Vleck paramagnet down to the lowest temperature when the crystal electric field split ground state is a singlet (e. g. in $\text{PrRhAl}_4\text{Si}_2^1$). There is a surge in the study of Pr compounds in recent times after the observation of heavy fermion superconductivity in $\text{PrOs}_4\text{Sb}_{12}$, $\text{PrV}_2\text{Al}_{20}$, and $\text{PrTi}_2\text{Al}_{20}$ at ambient or under pressure, originating from the quadrupolar Kondo order of Pr f -orbitals^{2,3}.

PrPd_2Ge_2 is a member of the well known large family of compounds crystallizing in the tetragonal ThCr_2Si_2 -type structure (space group $I4/mmm$, # 139). A previous report on polycrystalline sample provided evidence for an antiferromagnetic transition at 5 K⁵. Further, neutron diffraction indicated a magnetic cell three times larger than the chemical cell and the Pr moments aligned along the c -axis with a spontaneous magnetization of $\sim 2.0 \mu_B$ at 2 K⁵. Three possible configurations of the moments in the antiferromagnetic state, compatible with the tripling of the magnetic cell, were presented. However, the authors of that work felt that neutron diffraction on a single crystal was necessary to determine unambiguously the magnetic configuration. In the present work, we explore the magnetic properties of a single crystal of PrPd_2Ge_2 , using the techniques of magnetization, electrical resistivity and heat capacity. Our data on single crystalline sample suggest that the easy direction of magnetization may not lie exactly along the c -axis. The crystal electric field (CEF) analysis reveals an interesting possibility of metamagnetism at high fields ($\simeq 35$ T) along the $[001]$ direction due to the crossover among the split energy levels with magnetic field.

II. CRYSTAL GROWTH

We used the Czochralski method to grow a single crystal of PrPd_2Ge_2 , in a tetra-arc furnace, as the compound melts congruently. First, a homogeneous polycrystalline ingot, weighing ~ 10 gm was prepared by repeated arc melting of the high pure metals in the stoichiometric ratio 1 : 2 : 2, which was subsequently used as starting material for the crystal growth. To start with, a tungsten rod was used as seed to pull the single crystal

out of molten charge. The pulling speed was maintained at 10 mm/hour, after the initial necking and stabilization. In order to estimate the magnetic part of the heat capacity and to estimate the magnetic entropy, a polycrystalline sample of the non-magnetic LaPd_2Ge_2 was also prepared in a home built mono arc furnace.

To confirm the phase purity of grown crystal, a small portion of the specimen was subjected to powder x-ray diffraction (XRD). The XRD (not shown here for brevity) revealed a clear pattern without any impurity peaks suggesting the single phase nature of the grown crystal. A Le-bail fit was performed on the x-ray diffraction pattern and the lattice constants were estimated to be $a = 4.336(8) \text{ \AA}$ and $c = 10.050(8) \text{ \AA}$, respectively, which are in good agreement with the previously reported values^{4,5}. The composition of the crystal was further confirmed by energy dispersive analysis by x-ray (EDAX). In order to study the anisotropic physical properties, the grown single crystal was cut along the principal crystallographic directions *viz.*, [100] and [001] using a spark erosion cutting machine and back-reflection Laue diffraction. Well defined Laue diffraction spots together with the four fold symmetry ascertain the good quality of the grown single crystal.

III. MAGNETIC SUSCEPTIBILITY AND MAGNETIZATION

Magnetic susceptibility of PrPd_2Ge_2 shows a clear anomaly at $T_N = 5.1 \text{ K}$, with field parallel to [100] and [001] directions, respectively (see, Fig.1), in conformity with the reported T_N of polycrystalline sample. Similar to isotypic CePd_2Ge_2 ⁶, PrPd_2Ge_2 also exhibits a significant anisotropy in the magnetic susceptibility at low temperatures, measured in a field of 0.1 T. Magnitude of χ along [100] is smaller than that of [001], and remains nearly temperature independent in the antiferromagnetic state below T_N , marking it as the hard axis of magnetization, while χ along [001] increases sharply at lower temperature after exhibiting a cusp at T_N , unlike the conventional behaviour for a simple two sublattice antiferromagnet. The increase in the magnetic susceptibility along the [001] direction at temperatures below T_N reveals that the magnetic structure is complex as determined from the neutron diffraction data by Welter and Halich⁵.

The Curie-Weiss fit to the inverse susceptibility data gives $\mu_{\text{eff}} = 3.70 (3.76) \mu_B/\text{Pr}$, and $\theta_p = -14.9 (4.3) \text{ K}$ in [100] and [001] directions, respectively. μ_{eff} values are close to $3.58 \mu_B$, predicted by the Hund's rules for free Pr^{3+} . A negative value of θ_p corresponds

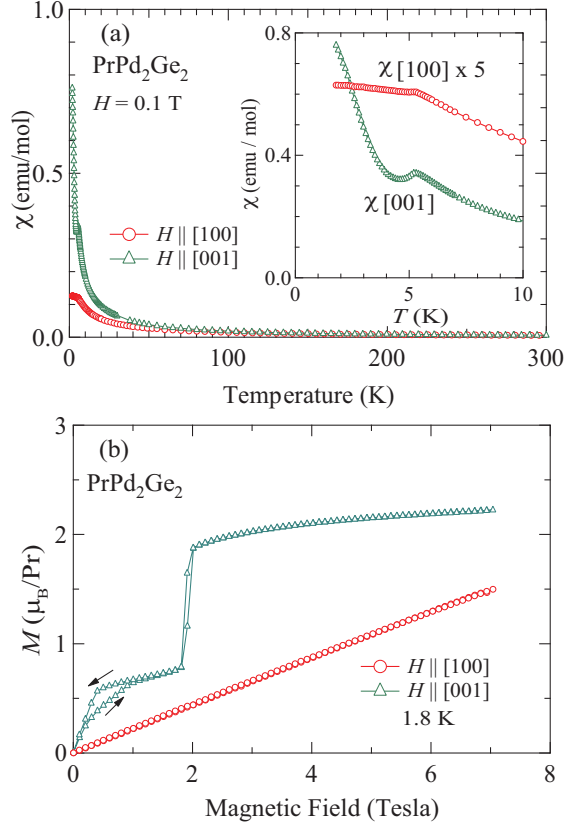


FIG. 1: (a) Magnetic susceptibility of PrPd_2Ge_2 between 1.9 and 300 K. Inset shows low temperature data on expanded scale, in which χ along [100] is multiplied by a factor of 5 to show its comparison with that of [001], (b) The isothermal magnetization data at 1.8 K along [100] and [001].

to antiferromagnetic correlations among Pr ions; however θ_p has a positive, albeit small, value along [001], which is tentatively ascribed to ferromagnetic interaction among the next nearest neighbours in the (001) plane.

The isothermal magnetization at 1.8 K along [100] varies linearly with field, which is in conformity with the basal plane being the hard plane of magnetization. On the other hand the magnetization along the tetragonal [001] direction, undergoes a distinct spin flip transition at 1.9 T. A change in the antiferromagnetic configuration presumably happens in the low field region (~ 1 T) as well which is marked by a distinct hysteresis. The magnetization attained at 7 T is 2.22 and $1.50 \mu_B/\text{Pr}$ for field parallel to [001] and [100] directions, respectively. These values are significantly lower than the saturation value of $3.20 \mu_B$ for Pr^{3+} ion corresponding to the total angular momentum quantum number $J = 4$ and Landé g-factor

($g_J = 4/5$). A higher magnetic field is required to populate all CEF split energy levels in order to attain the full moment value (see section VI). It may be noted that for a bipartite collinear antiferromagnet, the susceptibility along the easy axis gradually decreases to zero as the temperature is gradually decreased to zero. The isothermal magnetization should be nearly zero up to spin flop transition. We do not see such behavior in our single crystal. We believe our data show that the Pr moments do not lie parallel to [001] axis and the neutron diffraction results reported in Ref. 5 are oversimplified.

IV. ELECTRICAL RESISTIVITY

From the electrical resistivity data, recorded between 2 and 300 K, shown in Fig. 2, PrPd₂Ge₂ is metallic down to 2 K. The resistivity is anisotropic and exhibits higher values for the current density J parallel to [100] direction. Note that below T_N , for $J \parallel [100]$, a faster drop resulting from the loss of magnetic disorder scattering is observed. But, for $J \parallel [001]$, $\rho(T)$ shows an upturn at T_N . Such a feature observed in some antiferromagnets is generally attributed to a reduction in electron density caused by the opening of a gap (superzone gap) in the Fermi surface at T_N when the magnetic periodicity is incongruent with the periodicity of the chemical unit cell. Fig. 2(b) shows the data for $J \parallel [100]$ and $H \parallel [001]$. It is noticed that the decrease of resistivity below T_N becomes less prominent as the field increases such that at intermediate transverse field (1.40-2.05 T), a characteristic signature of superzone gap is observed (Fig. 2(b)). Whether the superzone gap persists to higher fields can be ascertained only by data taken at temperatures lower than 2 K. This interesting observation shows that in PrPd₂Ge₂, the superzone gap doesn't depend only on direction, but it is also a function of magnetic field. On the other hand, for $J \parallel [001]$ and $H \parallel [100]$, the zero field superzone gap persists at least up to 10 T (Fig. 2(c)). However, the overall magnitude of resistivity, the upturn at T_N and T_N decrease. It is to be mentioned here that the jump in the electrical resistivity at the superzone gap in zero field is very small, roughly estimated to be $0.12 \mu\Omega\cdot\text{cm}$ indicates Fermi surface gap is very small in this case. In order to estimate the magnitude of Fermi surface gapping, we followed the technique used by Mun et al.⁷ for YbPtBi by calculating the relative change in the conductivities using the relation: $(\sigma_n - \sigma_g)/\sigma_n$, where $\sigma_n(= 1/\rho_n)$ and $\sigma_g(= 1/\rho_g)$ are the conductivities of normal and the gapped states. The conductivity values obtained below and above the superzone

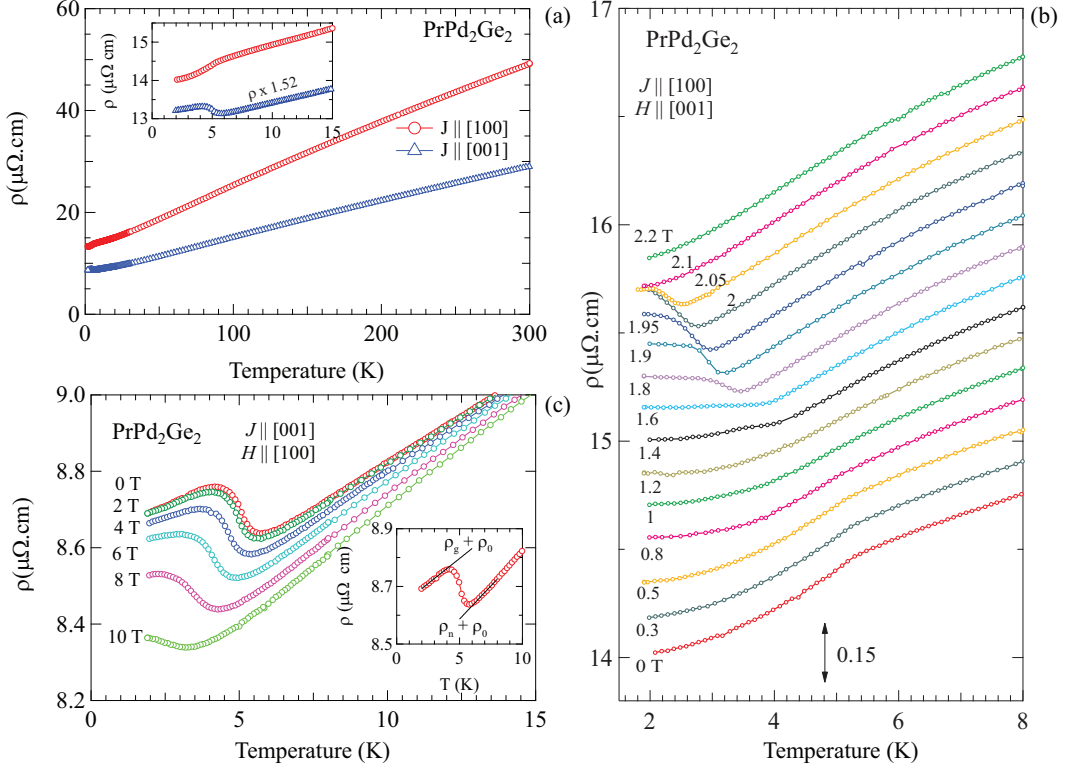


FIG. 2: (a) Variation of zero field electrical resistivity ρ with temperature, with current density J parallel to principal crystallographic directions in PrPd_2Ge_2 . Inset zooms up the low temperature part, for $J \parallel [001]$ direction the data is multiplied by 1.52 to show up in the same y -axis scale. (b) and (c) show the $\rho(T)$ data at selected transverse field in both configurations, respectively. Various iso-field traces of resistivity in (b) are shifted vertically for clarity. The inset in (c) shows the low temperature electrical resistivity for $J \parallel [001]$, the solid lines are linear fit to the resistivity data to estimate the ρ_n and ρ_g , the resistivities of the normal and the gapped state.

gap are shown in Table I. It is obvious from the table that the Fermi surface gapping is only 3% and it is almost constant for fields up to 4 T. In order to get more insight into the behaviour of the Fermi surface gapping, experiments down to low temperature are necessary.

V. HEAT CAPACITY

The heat capacity of PrPd_2Ge_2 and non magnetic reference compound LaPd_2Ge_2 measured between 1.9 K and 20 K, is shown in Fig. 3. The antiferromagnetic transition at 5.1 K is marked by a sharp peak. The low temperature anomaly observed on a polycrystalline

TABLE I: The electrical resistivity values obtained from the linear fit (refer to inset of Fig. 2(b)) to the electrical resistivity data at temperatures below and above the superzone gap in different magnetic fields. The last column gives the degree of Fermi surface gapping estimation.

Magnets Field (T)	Resistivity	Conductivity	Resistivity	Conductivity	$\Delta\sigma = \frac{\sigma_n - \sigma_g}{\sigma_n}$
	ρ_g ($\mu\Omega\cdot\text{cm}$)	$\sigma_g = 1/\rho_g$ ($\mu\Omega\cdot\text{cm}$) ⁻¹	ρ_n ($\mu\Omega\cdot\text{cm}$)	$\sigma_n = 1/\rho_n$ ($\mu\Omega\cdot\text{cm}$) ⁻¹	
0	8.6229	0.115970	8.3555	0.11968	0.03099
1.6	8.6294	0.11588	8.3600	0.11962	0.03126
2.0	8.6260	0.11593	8.3670	0.11952	0.03004
2.6	8.6165	0.11606	8.3558	0.11968	0.03025
4.0	8.6189	0.11602	8.3258	0.12011	0.03405

sample of PrPd₂Ge₂ by Welter and Halich⁵ at 3 K is not observed in our heat capacity data, indicating the good quality of our sample. The heat capacity of non magnetic iso-structural LaPd₂Ge₂ was subtracted from that of PrPd₂Ge₂, to estimate the contribution by Pr-4*f* electrons only (C_{4f}), assuming identical phonon contribution to the heat capacity in two compounds. Entropy S_{4f} was calculated by the same process as described for CePd₂Ge₂. A smooth extrapolation of $C(T)$ data below 1.9 K in PrPd₂Ge₂ was done as shown by the solid line in Fig. 3, to get an approximate value of the heat capacity at low temperatures for which the experimental data are not available. The error in the estimation of entropy due to extrapolation is at the most a few % of its true value. At T_N , S_{4f} is comparable to $R\ln 2$ corresponding to a doublet ground state with effective spin $S = 1/2$. Here R is the universal gas constant. From the C_{4f} values at higher temperatures, the CEF split levels have been derived, which is the subject of next section.

VI. CRYSTAL ELECTRIC FIELD ANALYSIS

A crystal electric field (CEF) analysis was performed on the magnetization and heat capacity data of PrPd₂Ge₂ to derive possible information about the crystal electric field level splittings. For the case of Pr ($J = 4, L = 5, S = 1$), CEF Hamiltonian can be expressed as,

$$\mathcal{H}_{\text{CEF}} = (B_2^0 O_2^0 + B_4^0 O_4^0 + B_4^4 O_4^4 + B_6^0 O_6^0 + B_6^4 O_6^4) + g\mu_B \mathbf{J} \cdot \mathbf{H}, \quad (1)$$

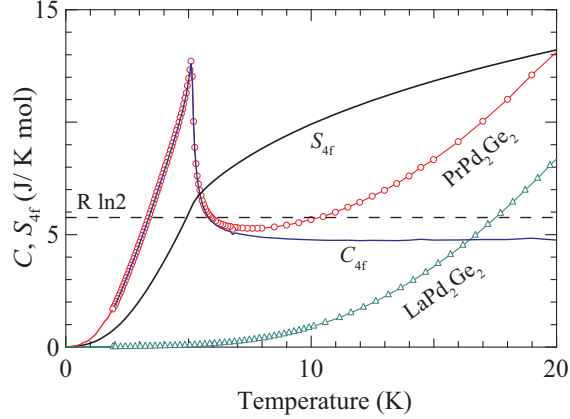


FIG. 3: Heat capacity (C) as a function of temperature in PrPd_2Ge_2 and non magnetic analog LaPd_2Ge_2 . The $4f$ contribution C_{4f} and calculated entropy S_{4f} are also shown on the same scale. Dashed horizontal line marks the $R \ln 2$ value of entropy, where R is the gas constant.

where B_l^m 's are CEF parameters and O_l^m 's are Steven's operators^{8,9}, respectively. Second term represents Zeeman energy in presence of magnetic field.

Pr is a non Kramer's ion (integral spin S). In the tetragonal \mathcal{D}_{4h} point symmetry, the CEF splits the 9 fold degenerate state of Pr^{3+} ion into two doublets and 5 singlets¹⁰. The compounds which exhibit singlet ground state are non magnetic (for instance the recently discovered $\text{PrRhAl}_4\text{Si}_2$)¹. Since PrPd_2Ge_2 orders at 5.1 K, the ground state is definitely doublet, as indicated strongly by the entropy (see above). Therefore, the excited states comprise of a ground state doublet and 5 singlets and another doublet at some higher energy.

After diagonalizing the $(2J + 1) \times (2J + 1)$ i.e. 9×9 dimensional matrices, the CEF parameters B_l^m , which fit the anisotropic susceptibility, isothermal magnetization (Fig. 4c) and Schottky heat capacity of PrPd_2Ge_2 , are listed in Table II and the computed curves are shown in Fig. 4 along with the experimental data. It may be noted that the heat capacity of both PrPd_2Ge_2 and LaPd_2Ge_2 was measured up to 80 K for this purpose. The ground state at zero magnetic field is an admixture of $|-1\rangle$ and $|+3\rangle$ pure states. There is a good degree of agreement between theory and observation, which gives credence to the correctness of the CEF parameters and energy levels derived from our analysis. However, advanced techniques like inelastic neutron scattering are required to confirm CEF splittings.

The main panel of Fig. 4(d) shows the calculated magnetization for applied field up to

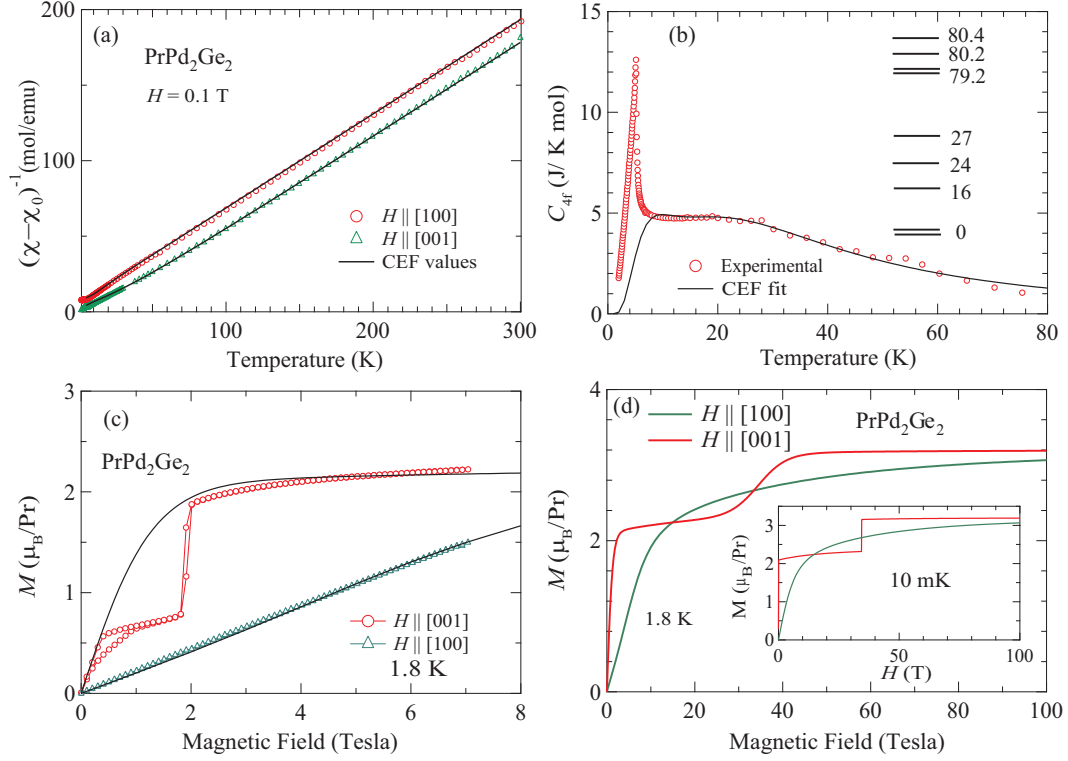


FIG. 4: A comparison of calculated (a) inverse susceptibility at 0.1 T, (b) heat capacity and (c) isothermal magnetization derived from CEF eigenstates and eigen values with the corresponding experimental data. (d) Calculated magnetization of PrPd₂Ge₂ up to 100 Tesla at 1.8 K (main panel) and at 10 mK (inset)

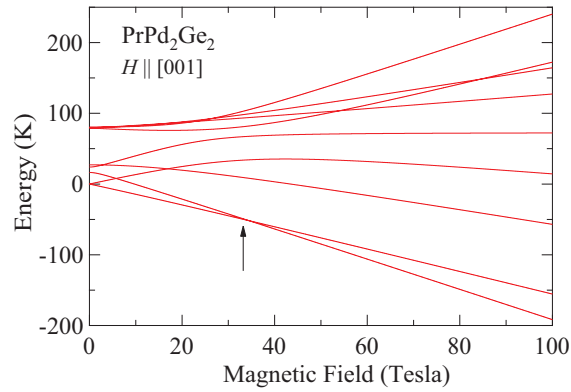


FIG. 5: Evolution of energy eigen values of CEF and Zeeman split Pr-energy levels with magnetic field along [001]-direction in PrPd₂Ge₂. Arrow marks the ground state level crossing, which leads to metamagnetism (cf. Fig. 4(d)).

TABLE II: CEF parameters, energy levels and the corresponding wave functions for PrPd₂Ge₂ at zero field.

CEF parameters									
B_2^0 (K)	B_4^0 (K)	B_4^4 (K)	B_6^0 (K)	B_6^4 (K)					
-1.1889	0.0147	0.0147	3.9490×10^{-4}	1.9220×10^{-5}					
$\lambda_{[100]} = 0.1569$ mol/emu, $\lambda_{[001]} = -1.28424$ mol/emu									
energy levels and wave functions									
E (K)	$ -4\rangle$	$ -3\rangle$	$ -2\rangle$	$ -1\rangle$	$ 0\rangle$	$ +1\rangle$	$ +2\rangle$	$ +3\rangle$	$ +4\rangle$
80.40	-0.2449	0	0	0	0.9381	0	0	0	-0.2450
80.23	0	0	0.7071	0	0	0	-0.7071	0	0
79.26	0	0	0	0.9507	0	0	0	-0.3101	0
79.26	0	-0.3101	0	0	0	0.9507	0	0	0
27.17	0	0	0.7071	0	0	0	0.7071	0	0
24.06	-0.7071	0	0	0	0	0	0	0	0.7071
16.37	0.6633	0	0	0	0.3464	0	0	0	0.6633
0	0	0.9507	0	0	0	0.3101	0	0	0
0	0	0	0	0.3100	0	0	0	0.9507	0

100 T. The magnetic field removes the degeneracy, and their energy evolution with magnetic field is governed by Eq. 1. The magnetization in [100] direction increases gradually with field and attains a marginally lower than full moment value of Pr ($3.2 \mu_B$) at 100 T where it has not yet achieved saturation. Interestingly, along the [001] direction, there is a meta magnetic jump at around 34 Tesla and the magnetization attains the theoretical saturation value at higher fields. The metamagnetic jump at 34 T has a different origin than the spin-flop transition that occurs at 1.9 T due to the change in the antiferromagnetic configuration with field. The metamagnetic jump at 34 T originates from the level crossing of the ground and the first excited CEF levels at that field (see Fig. 5) due to the dominance of Zeeman splitting over CEF splitting. When the magnetization is calculated for a temperature of 10 mK (inset of Fig. 4(d)), the metamagnetic transition due to level crossings is nearly vertical as one would expect it to be in the ground state, free of effects due to thermal fluctuations

at higher temperature. It would be interesting to measure the magnetization at higher fields to confirm the results of our CEF based calculations.

VII. CONCLUSION

The anisotropic magnetic properties of PrPd₂Ge₂ have been investigated by growing a single crystal, in a tetra-arc furnace. The phase purity and the crystal composition were confirmed by x-ray diffraction and EDAX. The transport and magnetic properties reveal large anisotropy along the two principal crystallographic directions *viz.*, [100] and [001]. The antiferromagnetic order is confirmed at $T_N = 5.1$ K. The increase in the magnetic susceptibility below T_N for $H \parallel [001]$, the easy axis direction, clearly reveals the complex magnetic structure of this compound. The electrical resistivity data of PrPd₂Ge₂ show the existence of anisotropic superzone gap which, interestingly, is dependent on both the crystallographic direction and applied magnetic field. The Néel temperature was found to decrease with increasing field, as expected for a typical antiferromagnet system. Our crystal field calculation explains the anisotropy in the magnetic susceptibility and magnetization of PrPd₂Ge₂. The energy levels determined from CEF analysis clearly explain the Schottky anomaly in the $4f$ -derived part of the heat capacity. The CEF levels in PrPd₂Ge₂ are comparatively low lying, which makes Zeeman interaction comparable to CEF splitting at a magnetic field of 34 Tesla leading to metamagnetic behaviour for $H \parallel [001]$ due to level crossing. Its confirmation by high field magnetization on a single crystalline sample is desirable.

* Electronic address: arvindmaurya.physics@gmail.com

¹ A. Maurya, R. Kulkarni, A. Thamizhavel, and S. K. Dhar, Solid State Commun. **240**, 24 (2016)

² E. Bauer, N. Frederick, P.-C. Ho, V. Zapf, and M. Maple, Phys. Rev. B **65**, 100506 (2002).

³ A. Sakai, and S. Nakatsuji, J. Phys. Soc. Jpn. **80**, 063701 (2011).

⁴ D. Rossi, R. Marazza, and R. Ferro, J. Less-Common Met. **66**, 17 (1979).

⁵ R. Welter, and K. Halich, J. Phys. Chem. Solids **67**, 862 (2006).

⁶ A. Maurya, R. Kulkarni, S. K. Dhar, and A. Thamizhavel, J. Phys.: Condens. Matter **25**, 435603 (2013).

- ⁷ E. D. Mun, S. L. Bud'ko, C. Martin, H. kim, M. A. Tanatar, J. -H.Park, T. Murphy, G. M. Schmiedeshoff, N. Dilley, R. Prozorov, and P. C. Canfield, *Phys. Rev. B* **87**, 075120 (2013).
- ⁸ M. T. Hutchings 1965 *Solid State Physics: Advances in Research and Applications* **Vol.16** edited by F. Seitz and B. Turnbull (New York: Academic) p.227.
- ⁹ K. W. H. Stevens *Proc. Phys. Soc. (London)* **Sect.A65**, 209 (1952).
- ¹⁰ W. A. Runciman, *Phil. Mag. Ser.* **81**, 1075 (1956).